Synthesis and Characterization of a New Family of Electroactive Alkali Metal Doped Mesoporous Nb, Ta, and Ti Oxides and Evidence for an Anderson Transition in Reduced Mesoporous Titanium Oxide

M. Vettraino,[†] M. Trudeau,[‡] and D. M. Antonelli*,[†]

Department of Chemistry and Biochemistry, University of Windsor, Windsor, Ontario, Canada N9B 3P4, and Emerging Technologies, Hydro-Québec Research Institute, 1800 Boul. Lionel-Boulet, Varennes, Quebec, Canada J3X 1S1

Received October 16, 2000

Recently we reported that mesoporous niobium oxide can be chemically reduced by Na-naphthalene while fully retaining its mesostructure. This was the first report of a molecular sieve acting as a stoichiometric electron acceptor. Herein we expand on the initial work by presenting a detailed study on Li-, Na-, K-, Rb-, and Cs-reduced samples of mesoporous Nb oxide, as well as Li-reduced mesoporous Ta and Ti oxides. While the Nb- and Ta-based materials fully retained their structure on reduction as determined by X-ray diffraction (XRD) and nitrogen adsorption, the Li-reduced Ti material retained high surface area and narrow pore size distribution, but lost its diffraction pattern, indicating an increased level of disorder in this material. X-ray photoelectron spectroscopy (XPS) and UV−visible reflectance spectroscopy revealed that all reduced mesoporous oxides studied have a similar electronic structure, corresponding to the presence of a disordered impurity band in the material lying between the valence band and the conduction band. Electron paramagnetic resonance (EPR) studies suggest that the electron in this impurity level is unpaired and best described as a free electron, only loosely bound to the alkali or transition metal. SQUID magnetometry showed that all reduced materials are paramagnetic, further confirming the presence of unpaired electrons in the structure. All materials in this study were insulating with the exception of the Li-reduced mesoporous Ti material, which was highly conducting, possibly due to an Anderson transition. Electrochemical studies on the unreduced mesoporous oxides demonstrated that while the Ta and Nb materials are capacitors with only a small degree of reversible electrochemical behavior in the bulk sample, the Ti material was an electrical conductor with fully reversible redox behavior.

1. Introduction

Since the discovery of mesoporous M41S silicates in 1992[1−6] there has been great interest in the synthesis of transition metal oxide analogues of these materials. While mesoporous silicates have flexible pore sizes from 20 to 100 Å, useful in applications requiring a catalytic support for processes where fast diffusion is essential, they lack the variable oxidation states and high surface acidity possessed by many transition metal oxides. This increased degree of chemical and electrochemical activity is necessary for many catalytic processes, especially those requiring flexible redox behavior and surface acid sites in order to be effective. While much work has been conducted on mesoporous silicates as catalytic supports,[7,8] adsorbents,[9,10] and hosts for intercalation of molecular guest species,[11,12] very little work has been done on applications of related transition metal oxide analogues. While some of these materials are inherently unstable to template removal,[13−15] there are a growing number of thermally robust mesoporous transition metal oxides which are readily accessible through mild and facile synthetic routes.[16] The applications of such materials to heterogeneous catalysis as well as to the fabrication of nanostructured electronic devices represents a new challenge in the field of materials engineering. Reliable preparative methods for mesoporous Nb,[17−20] Ta,[21] and

* Author to whom correspondence should be addressed.
[†] University of Windsor.
[‡] Hydro-Québec Research Institute.

(1) (a) Kresge, C. T.; Leonowicz, M. E.; Roth, W. J.; Vartuli, J. C.; Beck, J. S. *Nature* **1992**, *359*, 710. (b) Beck, J. S.; Vartuli, J. C.; Roth, W. J.; Leonowicz, M. E.; Kresge, C. T.; Schmitt, K. D.; Chu, C. T.-W.; Olson, D. H.; Shepard, E. W.; McCullen, S. B.; Higgins, J. B.; Schlenker, J. L. *J. Am. Chem. Soc.* **1992**, *114*, 10834.
(2) Firouzi, A.; Kumar, D.; Bull, L. M.; Besier, T.; Sieger, P.; Huo, Q.; Walker, S. A.; Zasadzinski, J. A.; Glinka, C.; Nicol, J.; Margolese, D.; Stucky, G. D.; Chmelka, B. F. *Science* **1995**, *267*, 1138.
(3) Chen, C.-Y.; Burkette, S. L.; Li, H.-X.; Davis, M. E. *Microporous Mater.* **1993**, *2*, 27.
(4) Tanev, P. T.; Chibwe, M.; Pinnavaia, T. J. *Nature* **1994**, *368*, 321.
(5) Behrens, P. *Angew. Chem.* **1996**, *108*, 565; *Angew. Chem., Int. Ed. Engl.* **1996**, *35*, 515.
(6) Antonelli, D. M.; Ying, J. Y. *Angew. Chem.* **1995**, *107*, 2202; *Angew. Chem., Int. Ed. Engl.* **1995**, *34*, 2014.
(7) Morey, M.; Davidson, A.; Eckert, H.; Stucky, G. *Chem. Mater.* **1996**, *8*, 486.
(8) Maschmeyer, T.; Rey, F.; Sankar, G.; Thomas, J. M. *Nature* **1995**, *378*, 159.
(9) Baker, J. M.; Dore, J. C.; Behrens, P. *J. Phys. Chem. B* **1997**, *101*, 6226.
(10) Morshige, K.; Nobuoka, K. *J. Chem. Phys.* **1997**, *107*, 6965.
(11) Moller, K.; Bein, T. *Chem. Mater.* **1998**, *10*, 2950.
(12) Wu, C.-G.; Bein, T. *Chem. Mater.* **1994**, *6*, 1109.
(13) Ciesla, U.; Demuth, D.; Leon, R.; Petroff, P.; Stucky, G.; Unger, K.; Schuth, F. *J. Chem. Soc., Chem. Commun.* **1994**, 1387.
(14) Huo, Q.; Margolese, D. I.; Ciesla, U.; Demuth, D. G.; Feng, P.; Gier, T. E.; Sieger, P.; Firouzi, A.; Chmelka, B. F.; Schuth, F.; Stucky, G. D. *Chem. Mater.* **1994**, *6*, 1176.
(15) Antonelli, D. M.; Trudeau, M. *Angew. Chem.* **1999**, *111*, 1555; *Angew. Chem., Int. Ed.* **1999**, *38*, 1471.
(16) Wong, M. S.; Mehnert, C. P.; Ying, J. Y. *Angew. Chem., Int. Ed.* **1999**, *38*, 56−77.
(17) Antonelli, D. M.; Ying, J. Y. *Angew. Chem.* **1996**, *108*, 461; *Angew. Chem., Int. Ed. Engl.* **1996**, *35*, 426.

10.1021/ic0011359 CCC: $20.00
Published on Web 03/22/2001

Ti[22] oxides, materials which fully retain their mesostructure to 400 °C, 600 °C, and 300 °C respectively, have been extensively developed, and these materials are now even commercially available. Mesoporous Zr oxides,[23−30] Hf oxide,[31] and Mn oxide,[32] the first semiconducting mesoporous oxide, have also been synthesized, and applications of these exciting new materials may soon be forthcoming. Because of the ready availability of these materials and their wealth of potential applications, it is anticipated that the next decade will see a substantial increase of interest in this area.

Recent advances in our group demonstrated that mesoporous Nb oxide can act as an electron acceptor while fully retaining its mesostructure.[33] This property is important from the standpoint of fabricating fast ion conduction channels for electrochemical cells and support materials for catalytic reduction of organic species. Hence, treatment of commercial mesoporous niobium oxide (surface area 947 $m^2\ g^{-1}$, pore size 22 Å) with up to 1 equiv of sodium naphthalene leads to new gray to black materials with surface areas ranging from 500 to 750 $m^2\ g^{-1}$, slightly reduced pore sizes, and an X-ray powder diffraction (XRD) pattern virtually identical to that of the parent oxide. These materials were found to be insulating, most likely due to localization of the electronic states in the disordered oxide framework. More recently, we showed that this electron acceptor property could be exploited so that mesoporous Nb oxide could act as a charge-balancing sheath stabilizing mixed oxidation state one-dimensional molecular phases of alkali fullerides,[34] cobaltocene,[35] and bis-benzene chromium.[36] The electronic and magnetic properties of these composites are highly unusual and demonstrate that the oxidizing ability of mesoporous niobium oxide can be used to create nonstoichiometric mixed oxidation state phases within the pore structure. Herein, to more fully understand properties of alkali metal reduced mesoporous transition metal oxide host−guest species, we present a full report on the synthesis, magnetic properties, and electronic behavior of mesoporous Nb oxide composites of Li, Na, K, Rb, and Cs—as well as Li-reduced mesoporous Ta and Ti oxides—including electrochemical reversibility studies and SQUID magnetometry measurements.

2. Experimental Section

Materials and Equipment. All chemicals were obtained from Aldrich unless otherwise stated. Samples of Nb-TMS1 with an HK pore size of 23 Å were obtained from Alfa-Aesar and used without further purification. The BET surface area of this material was 947 $m^2\ g^{-1}$, and the cumulative pore volume was 0.53 $cm^3\ g^{-1}$. The infrared (IR) spectrum showed no evidence of a hydrocarbon C−H stretch at ca. 2800 cm^{-1}. The XRD pattern for this material showed a peak at $d = 32$ Å. Mesoporous Ti and Ta oxides were also obtained from Alfa-Aesar and used without further purification. Trimethylsilyl chloride was obtained from Aldrich and distilled over calcium hydride. Nb-TMS1 samples were dried at 100 °C overnight under vacuum and then stirred with excess trimethylsilyl chloride in dry ether for 4−6 h under nitrogen. Nitrogen adsorption data was collected on a Micromeritics ASAP 2010. X-ray diffraction patterns (Cu Kα) were recorded in a sealed glass capillary on a Seimens D-500 θ-2θ diffractometer. All XPS peaks were referenced to the Carbon C-(C,H) peak at 284.8 eV and the data were obtained with a Physical Electronics PHI-5500 using charge neutralization. The conductivity measurements were recorded on a Jandel 4 point universal probe head combined with a Jandel resistivity unit. The equations used for calculating the resistivity were as follows for pellets of <0.1 mm thickness:

$$\rho = \left(\frac{\pi}{\log n^2}\frac{V}{I}\right)t$$

For pellets of >0.5 mm thickness the following equation is used:

$$\rho = 2\pi(S)\frac{V}{I}$$

where ρ = resistivity; $\pi/(\log n^2)$ = sheet resistivity; V = voltage; I = current; t = thickness of the pellet; S = the spacing of the probes (0.1 cm). The band gaps were recorded from powder UV−visible spectra collected on an Ocean Optics S2000 fiber optics spectrometer equipped with an Analytical Instrument Systems Light Source emitter with a tungsten halogen lamp and an Ocean Optics UV 0.4 mm, 2M reflection probe. Electron paramagnetic resonance (EPR) spectra were recorded at the temperature of liquid nitrogen on an X-band Bruker ESP 300E spectrometer equipped with a microwave counter, an NMR magnetometer, and an electromagnet capable of providing a magnetic field range from 50 G to 15 kG. All elemental analysis data was obtained from Galbraith Laboratories, Knoxville, TN (inductively coupled plasma). Inductively coupled plasma techniques were employed to obtain specific percentages of metals in the samples. Cyclic voltammetry measurements were made in a three-electrode cell with an EG&G model 283 potentiostat/galvanostat employing model 270 Electrochemistry Analysis softwear (Princeton Research Corp.). A saturated calomel electrode was used as the reference electrode and was separated from the working electrode chamber by a Luggin capillary, and the counter electrode was platinum wire.

Synthesis. To a suspension of the alkali metal (caution) in tetrahydrofuran (THF) in an inert atmosphere glovebox was added 1.0 equiv of naphthalene. The mixture was stirred until the solid was completely consumed. At this point the solution was a deep brownish black color. On the basis of 53% Nb as determined from the elemental analysis data, 1.0 equiv of the trimethylsilated Nb-TMS1 was added to the tetrahydrofuran solution. The solution immediately lightened, indicating absorption of the alkali, and the mesoporous solid went from a light white to fawn color to a deep gray-black. After 1 h of additional stirring, the reduced material was collected by suction filtration and washed several times with THF. The materials were then dried in vacuo at 10^{-3} Torr on a Schlenk line until the vacuum gauge showed that all condensable volatiles had been removed. Elemental analysis of this new material showed values of 46.35% Nb, 8.11% C, 2.18% H, 0.95% Si, and 7.46% Na. All other reduced samples in this study were prepared in a directly analogous fashion. The Nb-based materials are gray to black in color, the Ta-based materials, brownish-gray, and the Ti-based materials, deep blue. The elemental analysis results are as follows.

1.0 Li-Nb: 44.24% Nb, 3.24% Li, 9.40% C, 1.49% H, <0.5% N, 1.99% Si. **1.0 Na-Nb:** 41.31% Nb, 10.85% Na, 7.18% C, 1.28% H,

(18) Antonelli, D. M.; Nakahira, A.; Ying, J. Y. *Inorg. Chem.* **1996**, *35*, 3126.
(19) Antonelli, D. M. *Microporous Mesoporous Mater.* **1999**, *30*, 209.
(20) Antonelli, D. M.; Ying, J. Y. *Curr. Opin. Colloid Interface Sci.* **1996**, *1*, 523.
(21) Antonelli, D. M.; Ying, J. Y. *Chem. Mater.* **1996**, *8*, 874.
(22) Antonelli, D. M. *Microporous Mesoporous Mater.* **1999**, *30*, 315.
(23) Reddy, J. S.; Sayari, A. *Catal. Lett.* **1996**, *38*, 219.
(24) Ciesla, U.; Schacht, S.; Stucky, G. D.; Unger, K.; Schuth, F. *Angew. Chem.* **1996**, *108*, 597; *Angew. Chem., Int. Ed. Engl.* **1996**, *35*, 541.
(25) Ciesla, U.; Fröba, M.; Stucky, G.; Schüth, F. *Chem. Mater.* **1999**, *11*, 227.
(26) Antonelli, D. M. *Adv. Mater.* **1999**, *11*, 487.
(27) Wong, M. S.; Antonelli, D. M.; Ying, J. Y. *Nanostruct. Mater.* **1997**, *9*, 165.
(28) Wong, M. S.; Ying, J. Y. *Chem. Mater.* **1998**, *10*, 2067.
(29) Mamak, M.; Coombs, N.; Ozin, G. *Adv. Mater.* **2000**, *12*, 198.
(30) Hudson, M. J.; Knowles, J. A. *J. Chem. Mater.* **1996**, *6*, 89.
(31) Liu, P.; Liu, J.; Sayari, A. *J. Chem. Soc., Chem. Commun.* **1997**, 577.
(32) Tian, Z. R.; Wang, J. Y.; Duan, N. G.; Krishnan, V. V.; Suib, S. L. *Science* **1997**, *276*, 926.
(33) Vettraino, M.; Trudeau, M.; Antonelli, D. M. *Adv. Mater.* **2000**, *12*, 337.
(34) Ye, B.; Trudeau, M.; Antonelli, D. M. *Adv. Mater.*, in press.
(35) (a) Murray, S.; Trudeau, M.; Antonelli, D. M. *Adv. Mater.* **2000**, *12*, 1339. (b) Murray, S.; Trudeau, M.; Antonelli, D. M. *Inorg. Chem.*, in press.
(36) He, X.; Trudeau, M.; Antonelli, D. M. *Adv. Mater.* **2000**, *12*, 1036.

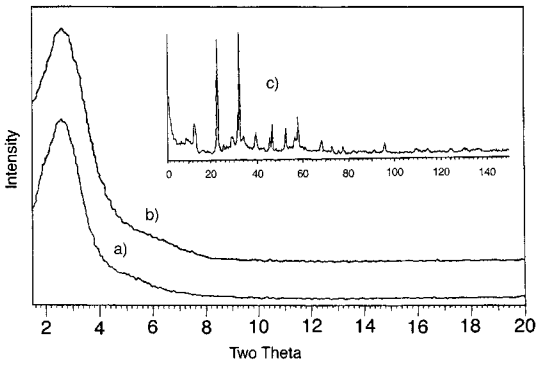

Figure 1. XRD of (a) a sample of Nb-TMS1 with a 22 Å pore size treated with trimethylsilyl chloride, (b) sample in part a treated with 1.0 equiv of Na-naphthalene, and (c) sample in part a treated with 2.0 equiv of Na-naphthalene showing high-angle reflections.

<0.5% N, 2.17% Si. **1.0 K-Nb:** 41.69% Nb, 15.48% K, 3.48% C, 0.96% H, 0.5% N, 1.88% Si. **1.0 Rb-Nb:** 39.10% Nb, 25.38% Rb, 4.08% C, 0.85% H, <0.5% N, 1.06% Si. **1.0 Cs-Nb:** 29.63% Nb, 32.57% Cs, 2.99% C, 0.65% H, <0.5% N, 2.51% Si. **1.0 Li-Ti:** 34.46% Ti, 4.35% Li, 12.90% C, 1.97% H, <0.5% N, 1.58% Si. **1.0 Li:Ta:** 59.10% Ta, 1.88% Li, 8.93% C, 1.47% H, <0.5% N, 1.68% Si.

3. Results and Discussion

3.1. Synthesis. A sample of mesoporous niobium oxide with an HK pore size of 22 Å and a surface area of 947 m^2 g^{-1}, displaying a peak in the XRD at $d = 32$ Å, when treated with 1.0 equiv of Na-naphthalene in THF yielded a sample with a virtually identical XRD pattern, indicating retention of the mesostructured framework, and a surface area of 449 m^2 g^{-1} and a pore size of 21 Å.[33] Figure 1 shows XRD patterns for a sample of trimethylsilated Nb-TMS1 with a pore size of 22 Å (a) and the same sample after treatment with 1.0 equiv of Na-naphthalene (b). The slight reduction in pore size is consistent with partial filling of the pores with Na-bound THF as previously described. The surface area monotonically decreases with Na-loading in full accordance with the increased density of the sample. Elemental analysis of the reduced samples generally showed an increase in carbon content of 2−3% with respect to the ca. 5% present in the starting material due to the trimethylsilyl groups on the walls of the mesostructure. This further supports the presence of Na-bound THF in the pores of the system. Samples that were not treated with trimethylsilyl chloride prior to treatment with alkali generally lost their XRD diffraction pattern upon reduction and possessed surface areas of less than 50% of the values of the starting mesoporous oxide, possibly due to the reduction of surface water to free hydroxide and the reductive deprotonation of Nb−OH groups to nucleophilic Nb oxo anions. Over the course of our investigations it was found that mesoporous niobium oxide is sensitive to basic media and rapidly loses its structure on pH values in excess of 9. This sensitivity to base is reflected in the reaction of Nb-TMS1 with Na-benzophenone, a radical anion reducing agent with the negative charge centered at oxygen. The replacement of naphthalene with benzophenone in this case leads to loss of structure and greatly reduced surface areas as determined by XRD and nitrogen adsorption. We attribute this to the nucleophilic and basic character of the oxygen anion in this reagent. The sensitivity of Nb-TMS1 to reactive oxygen species is further demonstrated by the reaction with hydrogen peroxide which leads to complete loss of the mesostructure as determined by a drop in the surface area from 700 to 1000 m^2/g to less than 50 m^2/g. Once synthesized, samples of sodium-reduced Nb-TMS1 are extremely air sensitive and rapidly lose their structure on air oxidation, possibly due to the buildup of nucleophilic oxygen species in the structure after exposure to air and subsequent reduction of water and dioxygen. Figure 1c shows the XRD pattern of the material from Figure 1a after treatment with 2.0 equiv of Na-naphthalene. The loss of the peak at $d = 32$ Å and emergence of new peaks at higher angle demonstrate that excess Na-naphthalene leads to complete degradation of the mesostructure and formation of a new phase or phase mixture. We were unable to find a satisfactory match in the JCPDS data file for the diffraction pattern of this material, indicating that this is possibly a new phase of reduced Na−Nb oxide. The BET surface area of this material as determined by nitrogen adsorption was 43 m^2 g^{-1}. This indicates that loading levels in excess of 1.0 equiv of alkali lead to degradation of the mesostructure and formation of a mixed-phase material

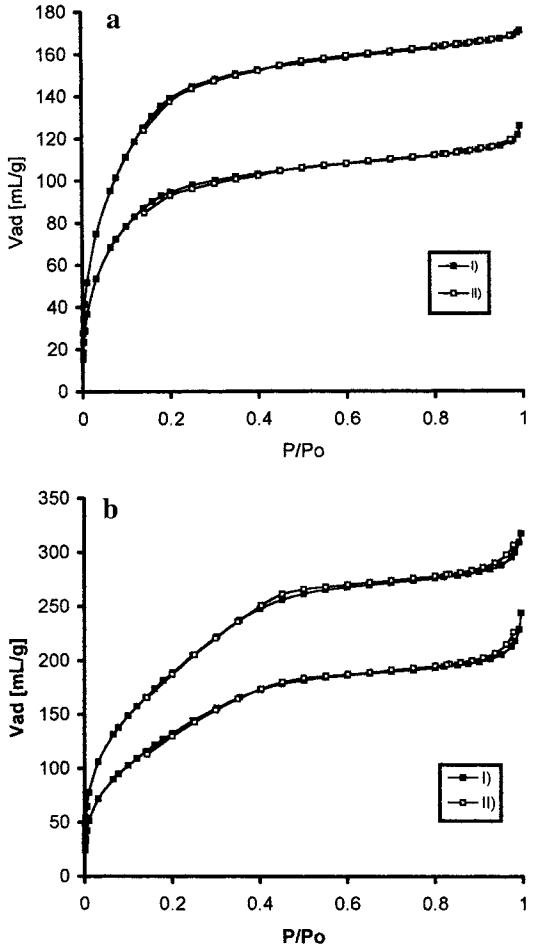

Figure 2. Nitrogen adsorption isotherms of (a) a sample of Ta-TMS1 treated with trimethylsilyl chloride (upper) and the same sample after treatment with 1.0 equiv of Li-naphthalene (lower) and (b) a sample of phosphate-free Ti-TMS1 (upper) and the same sample after treatment with 1.0 equiv of Li-naphthalene (lower).

In the course of our studies we extended this new family of reduced mesoporous materials to include oxides of Ta and Ti to probe the effect of changing the transition metal in the mesoporous framework on stability of the material to reduction and subsequent electronic properties of the reduced species. While tantalum oxides are of interest because of their extreme electrical resistivity, titanium oxides have applications in a wide range of catalytic and photochemical processes. In accordance with the procedure described for reduction of Nb-TMS1, samples of Ta-TMS1 and phosphate-free Ti-TMS1 were reduced in THF with 1.0 equiv of Li-naphthalene to yield corresponding reduced oxides. Li was used in this case because of the potential

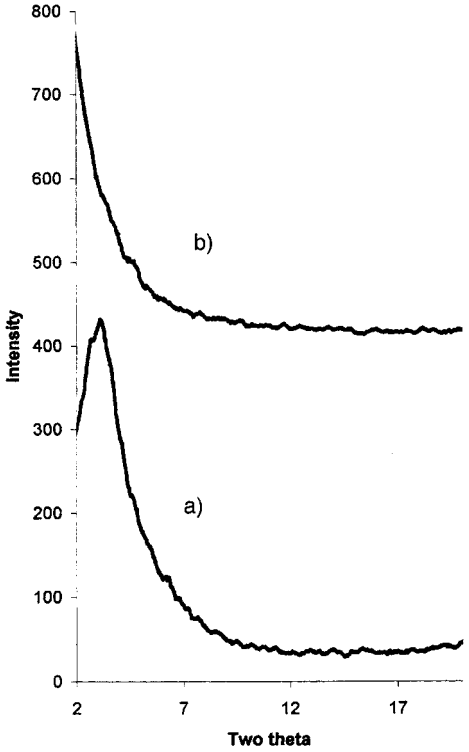

Figure 3. XRD patterns of reduced samples from (a) Figure 2a and (b) Figure 2b.

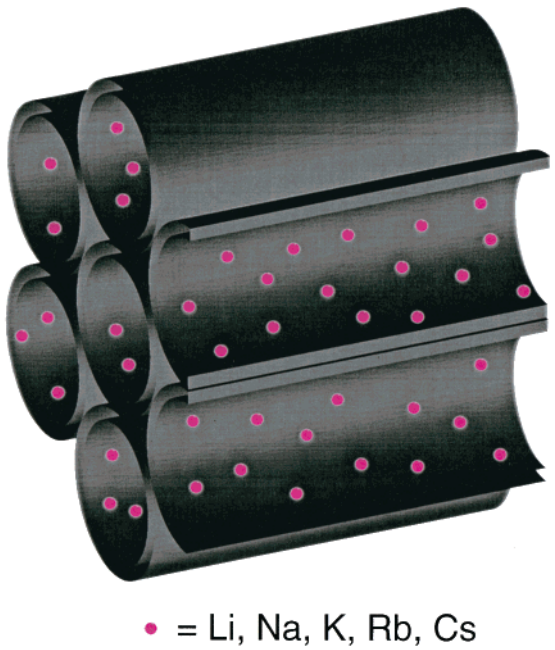

Figure 4. Schematic representation depicting random distribution of alkali metals in the structure of mesoporous oxides (Ta, Nb, Ti) reduced with alkali metal (Li, Na, K, Rb, Cs).

application of mesoporous oxides as fast ion conduction channels in Li-based batteries.[37] Panels a and b of Figure 2 show the nitrogen adsorption isotherms for trimethylsilated samples of Ta-TMS1 (BET surface area = 538 m^2 g^{-1}, HK pore size = 23 Å, d = 32 Å) and Ti-TMS1 (BET surface area = 793 m^2 g^{-1}, HK pore size = 25 Å, d = 38 Å) respectively before and after treatment with 1.0 equiv of Li-naphthalene calculated on the basis of ca. 38% Ti and ca. 57% Ta showing the expected reduction of surface area due to the increase of the sample density with increase of alkali content. The reduced Ti sample had a BET surface area of 517 m^2 g^{-1} and an HK pore size of 24 Å while the Ta material had a surface area of 359 m^2 g^{-1} and a pore size of 22 Å. Figure 3 shows the XRD patterns for the Li-reduced Ta and Ti materials and indicates that the Ta-based material (Figure 3a) fully retained its mesostructure, even after exposure to air and reoxidation, while the Ti material (Figure 3b) lost its diffraction pattern on treatment with alkali. This is consistent with a more disordered pore structure in the reduced Ti-based material than in the corresponding Nb and Ta materials and further suggests that the order of stability of the mesostructures to reduction is Ta > Nb ≫ Ti. This is in accord with previous studies on these materials regarding the thermal and hydrothermal stability of the untreated samples. Figure 4 shows a schematic representation of these materials, depicting the impregnation of the pore structure by the alkali metal, here shown in pink.

3.2. Conductivity and UV. Conductivity measurements on all compositions of reduced Nb and Ta materials studied gave values of less than 10^{-7} ohm^{-1} cm^{-1}. A comparison between the reduced Nb materials and known semiconducting crystalline Nb(IV) oxides has been discussed previously,[33] and the lower than expected conductivities in our materials attributed to Anderson localization effects[38,39] due to the amorphous nature of the walls of the mesostructured oxide. Grain boundary effects between adjacent grains of these nanostructured materials may also be at play. The Li−Ti material, however, gave conductivity values of 10^{-6} ohm^{-1} cm^{-1}, demonstrating that localization effects in this material do not dominate over electron mobility as they do in the Nb and Ta materials. This will be discussed in further detail in the next section. Since changing the size of a cation can often lead to changes in physical properties of a material, we reduced samples of Nb-TMS1 with an HK pore size of 23 Å and a surface area of 947 m^2 g^{-1} with the series of M′-naphthalene reagents (M′ = Li, Na, K, Rb, Cs). The HK pore sizes of all materials were in the range 19−21 Å, and the BET surface areas decreased monotonically with increasing molecular weight of the alkali metal from 549 m^2 g^{-1} for Li to 342 m^2 g^{-1} for Cs. XRD patterns for all materials in this series showed a peak at ca. d = 32 Å. These data support retention of the mesostructure for these new reduced oxides. UV reflectance studies on all reduced materials, including the Li−Ti and Li−Ta materials discussed above, showed broad absorbancies at 220−250 nm for the M−O sp valence band (VB) to conduction band (CB) transition (ca. 3.3 eV), in agreement with previous studies by Stone and Davis on these and related materials.[40] In addition to this, all samples showed a broad absorbance of much weaker intensity centered at ca. 580 nm, corresponding to an energy of 2.1 eV. In the Na-reduced Nb-based system this absorbance was previously assigned to a Nb4d−Na3s impurity band. Thus, in accordance with this previous work, we attribute these related absorbances to an Mnd−M′n′s band [M = Ti, Nb, Ta; n = 3(Ti), 4(Nb), 5(Ta)″; M′ = Li, Na, K, Rb, Cs; n′ = 2(Li), 3(Na), 4(K), 5(Rb), 6(Cs)]. In all cases the Nb- and Ta-based materials had conductivity values of less than 10^{-7} ohm^{-1} cm^{-1}, indicating that substitution of the alkali had no observable effect on the conductivity of the material and that the different behavior of the Li−Ti system is most likely due to the different electronic structure of the Ti mesostructure as compared to that

(37) MacFarlane, D. R.; Huang, J.; Forsyth, M. *Nature* **1999**, *402*, 792.
(38) Cox, P. A. *The Electronic Structure and Chemistry of Solids*; Oxford University Press: New York, 1987.
(39) Cheetham, A. K.; Day, P. *Solid State Chemistry, Compounds*; Oxford University Press: New York, 1992.
(40) Stone, V. F., Jr.; Davis, R. *Chem. Mater*. **1998**, *10*, 1468.

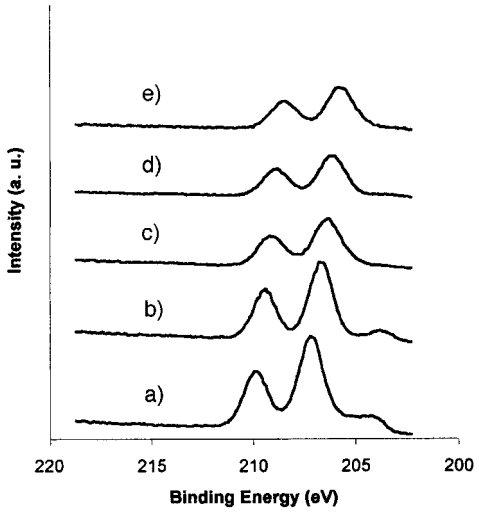

Figure 5. The Nb 3d region of the XPS spectrum of samples of Nb-TMS1 reduced with 1.0 equiv of (a) Li-naphthalene, (b) Na-naphthalene, (c) K-naphthalene, (d) Rb-naphthalene, and (e) Cs-naphthalene showing the $^3/_2$,$^5/_2$ peaks.

of the Nb and Ta materials, and not the substitution of different alkali metals into the respective mesostructures.

3.3. XPS Studies. X-ray photoelectron spectroscopy (XPS) was conducted on all samples to measure the binding energies of the core electrons and so deduce the degree of reduction in the walls of the mesostructure. In previous work[33] we showed that reduction of Nb-TMS1 with 0.2, 0.6, and 1.0 equiv of Na-naphthalene led to a gradual shift to lower binding energy of the Nb 3d $^3/_2$,$^5/_2$ peaks from 206.8 eV for the unreduced sample to 205 eV for the sample reduced with 1.0 equiv. This is consistent with a gradual change of oxidation state from Nb-(V) to Nb(IV) with increased Na loading. Since the shift of XPS peaks depends on local environment of the nucleus as well as oxidation state, it was necessary to compare the Nb 3d positions between Nb-TMS1 materials reduced with different alkali metals in order to gauge the degree of ion size on peak position. This trend is important for future studies on composites of this material so that the Nb 3d peak positions can be readily used to deduce the mean oxidation state of the Nb walls. Figure 5 shows the XPS spectrum of the Nb 3d region of samples of Nb-TMS1 of a 22 Å pore size and 947 m^2 g^{-1} reduced with 1.0 equiv of Li, Na, K, Rb, and Cs. For each step downward within group 1 of the periodic table the $^3/_2$,$^5/_2$ peaks move to the right by roughly 0.4 eV, demonstrating that changing the alkali metal has a tendency to move the peaks to a lower binding energy as the alkali metal increases in size and becomes more electropositive. This is consistent with an increase of electron density at the Nb center as the larger alkali metal is less able to stabilize the negative charge. As previously noted, this system shows just one peak for samples of intermediate oxidation state, indicating that there is an averaging on the XPS time scale of adjacent Nb(IV) and Nb(V) sites or that the amorphous nature of the material gives a broad distribution of overlapping states, either of which would lead to the observation of just one peak. The samples reduced with Li and Na shows a small hump at lower binding energy at roughly the same position expected for either metallic Nb, indicating that in this case a small degree of decomposition to the metal occurred, possibly due to increased oxophilicity of Li over the other alkali metals, making Li-naphthalene better able to reduce the oxygenated niobium center to oxidation states lower than IV because of coordination of the Li to the Nb-bound oxygen. Figure 6 shows the Nb 3d $^3/_2$,$^5/_2$ region for the same sample of mesoporous niobium oxide

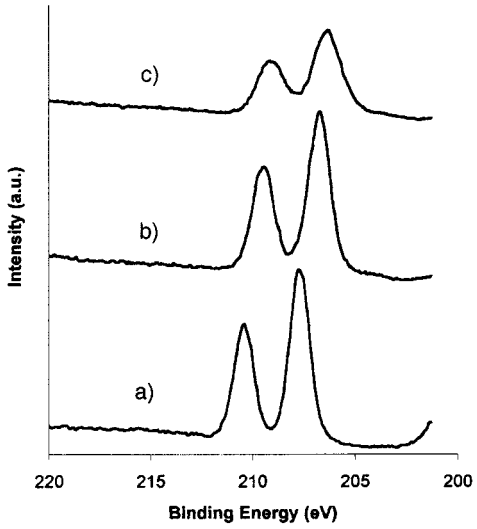

Figure 6. The Nb 3d region of the XPS spectrum of samples of Nb-TMS1 reduced with (a) 0.2 equiv of K-naphthalene, (b) 0.6 equiv of K-naphthalene, and (c) 1.0 equiv of K-naphthalene showing the $^3/_2$,$^5/_2$ peaks.

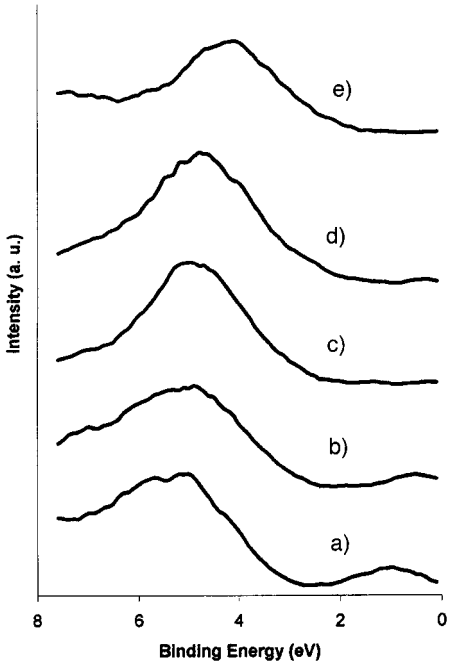

Figure 7. The valence region near the Fermi level of samples of Nb-TMS1 reduced with 1.0 equiv of (a) Li-naphthalene, (b) Na-naphthalene, (c) K-naphthalene, (d) Rb-naphthalene, and (e) Cs-naphthalene.

reduced with 0.2, 0.6, and 1.0 equiv of K-naphthalene. This region is of special interest in the study of K_3C_{60} intercalates studied by our group as the degree of reduction of the mesostructure walls in this system is important in helping to determine the mean oxidation state of the C_{60} units in the structure.[34] The $^3/_2$,$^5/_2$ peak positions move monotonically with degree of reduction from 206.8 to 205 eV as previously reported for the Na-reduced Nb materials, demonstrating that although peak positions at a given dopant concentration move to lower binding energy with increasing molecular weight of the alkali, the trend of decreasing binding energy of the 3d electrons with increasing dopant concentration is similar from one alkali metal series to another. Figure 7 shows the Nb−O sp valence region near the Fermi level of these samples, revealing a distance of roughly 3.0 eV to the Fermi level as observed for the Na-reduced samples. Specific assignments of these peaks is difficult because

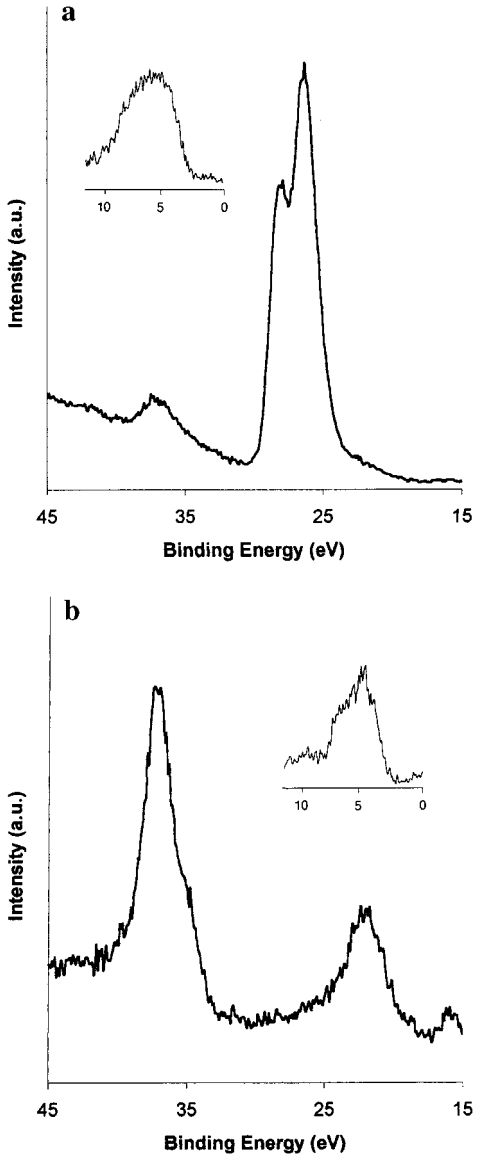

Figure 8. The XPS spectrum of Li-reduced samples from (a) Figure 2a showing the Ta 4f region and (b) Figure 2b showing the Ti 3p region. The inset in each shows region near the Fermi level in each sample.

of the high-energy nature of XPS and the subtle electronic interactions at play near the Fermi level. The small hump in the Li-reduced samples near the Fermi level is consistent with a small amount of a metallic species, Li or possibly Nb as supported by the small hump in the Nb 3d region at lower binding energy, in the mesostructure. Figure 8a shows the Ta 4f $^{5}/_{2},^{7}/_{2}$ region of the Li-reduced sample of mesoporous Ta oxide from Figure 2a. The $^{7}/_{2}$ peak falls at 26.1 eV compared to that in the unreduced trimethylsilated material at 26.9 eV. This is consistent with reduction of the Ta center by the Li reagent. Figure 8b shows the Ti 3p $^{1}/_{2},^{3}/_{2}$ region of the sample of mesoporous Ti oxide treated with 1.0 equiv of Li-naphthalene from Figure 2b. The $^{1}/_{2}$ peak appears at 36.8 eV as compared to 37.9 eV in the unreduced trimethylsilated material, again fully consistent with reduction of the Ti center by Li-naphthalene. The insets of both panels a and b in Figure 8 show the valence region near the Fermi level in each material, corresponding to a distance of ca. 3.0 eV from the M-sp valence band to the Fermi level, as previously noted for the reduced Nb materials.

Figure 9 shows a schematic representation of the energy levels of reduced mesoporous oxides as suggested by our data. The

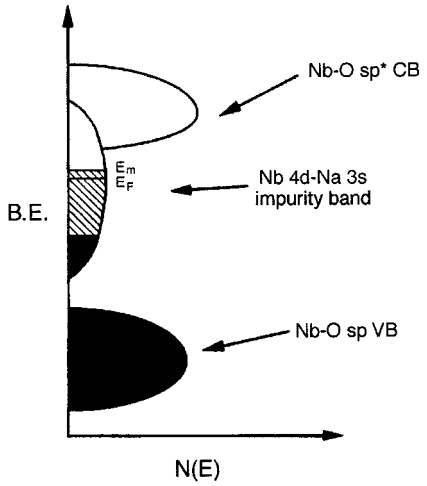

Figure 9. Energy level diagram of alkali-reduced M-TMS1 (M = Ta, Nb, Ti). The alkali electron resides in an *ns*(alkali)−M*n*′d impurity band between the valence and conduction bands of the mesostructure. E_F denotes the Fermi level while E_m represents the mobility edge. Black areas are filled with electrons while the area marked by grid lines represents a region of localized states extending down into the black filled levels of the impurity band.

band gap (distance from the VB to the CB) is 3.3 eV as previously described, while the distance from the shaded filled levels of the impurity band to the conduction band is 2.1 eV. For the sake of simplicity, the higher unfilled levels of the impurity band in Figure 9 are shown overlapping with the conduction band, although our data does not allow us to determine the exact relationship between these two bands in this energy region. The XPS spectrum of all materials suggests a distance of ca. 3.0 eV from the VB to the Fermi level. The d-based impurity band is shown divided into several regions as necessitated by Anderson localization within this band, a phenomenon associated with n-doped amorphous oxides such as Na_xWO_3.[38] While other localization effects related to the balance between electron repulsion (U) and bandwidth (W) of the impurity band could also be at play in our systems, these effects are rare in early metal oxides because of the large bandwidths of the d-states and smaller amount of d-electrons within the band as compared to the middle and late metal oxides. In Anderson localization the electrons are localized due to the amorphous nature of the solid and the position of the Fermi level (E_F in the figure) below a mobility edge (E_m) within the band. Above the mobility edge in our system lie continuous d-states while below the mobility edge are localized d-states of random potential. This latter region is depicted with grid lines in the figure. An Anderson transition to a metallic state occurs when enough dopant is added to begin filling the continuous states above the mobility edge. In such a case the Fermi level moves to a position above the mobility edge. In the reduced Ta-TMS1 and Nb-TMS1 materials the lack of conductivity and amorphous nature of the oxide suggest an electronic structure dominated by Anderson localization. Since the Li−Ti material is conducting, other electronic effects must be at play. The reason for this change in behavior from Nb and Ta to Ti is not fully understood as conductivity in this material may arise in three different ways: (1) an electron may be promoted from the Li2s−Ti3d impurity band of the material to the Ti−O sp* conduction band as in an n-doped semiconductor; (2) the filled levels of the impurity band may overlap with the Ti−O sp* conduction band as proposed previously for n-doped samples of $SnSe_2$ (this would correspond to the black region in the impurity band in Figure 9 overlapping with the sp*

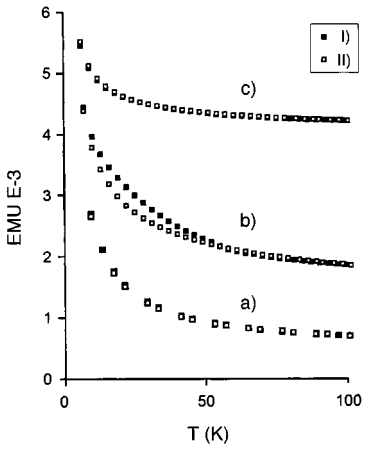

Figure 10. SQUID plot of magnetic susceptibility versus temperature for (a) a sample of Nb-TMS1 reduced with 1.0 equiv of Li-naphthalene; (b) a sample of Ti-TMS1 reduced with 1.0 equiv of Li, and (c) a sample of Ta-TMS1 reduced with 1.0 equiv of Li.

conduction band), thus allowing electrons to move through the conduction band without having to be promoted; (3) an Anderson transition within the impurity band may occur, allowing conductivity pathways within this d-based level without the influence of any higher energy electronic states such as the conduction band. Possibility 2 can be readily ruled out on the basis of the 2.1 eV distance from the highest filled levels of the impurity band to the conduction band in this material as determined by UV spectroscopy. For this explanation to be plausible the energy distance between these regions would have to be zero, and no absorbance due to an impurity band would be visible. While our data does not allow us to unambiguously distinguish between the first and third pathways, the fact that the 2.1 eV distance from the filled impurity levels to the conduction band in the reduced Ti material is very close to that in the reduced Ta-TMS1 and Nb-TMS1 materials suggests that there should be little or no difference in conductivity in these materials if this mechanism is at work. Also, the distance to the Fermi level in each material is almost identical (ca. 3.0 eV), lending further support to the picture that the electronic structure and relative energy spacings between bands in these materials are very similar. Thus, our data tends to support the picture that conductivity occurs through the high-lying continuous d-states in the impurity band and that an Anderson transition occurs in the Ti system, but not in the Ta or Nb system. This implies that the ratio of localized to continuous states in this band is greater for the group V materials than for the Ti material.

3.4. SQUID Magnetometry and EPR Studies. Superconducting quantum interference device (SQUID) magnetometry on all samples demonstrated that the reduced Nb, Ta, and Ti materials were all paramagnetic with standard Currie Weiss behavior observed as the sample was warmed from 4 to 100 K. The plot of the magnetic susceptibility versus temperature of samples of mesoporous Nb, Ta, and Ti oxide reduced with 1.0 equiv of Li is shown in Figure 10. At 4.0 K the values for the magnetic susceptibility were in the range $2.5-5.5 \times 10^{-3}$ emu/g. Although it may be expected that the lighter materials would have a greater degree of unpaired electrons per gram on the basis of molar mass leading to a trend for increasing M at 4.0 K of Ta < Nb < Ti, the fact that there is no obvious pattern to these data shows that varying degrees of spin pairing and metal−metal bonding interactions are at play. This would change the amount of unpaired electrons in each system thus influencing the relative degrees of paramagnetism. Room temperature electron paramagnetic resonance (EPR) spectra of all reduced

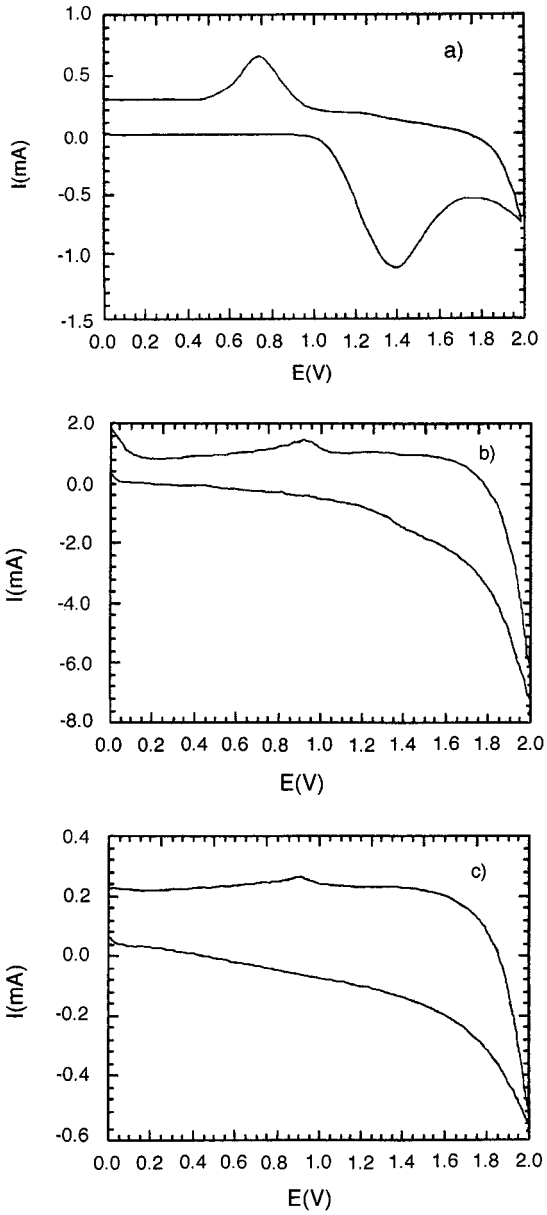

Figure 11. Cyclic voltamograms at 100 mV for trimethylsilated samples of M-TMS1: (a) M = Ti, (b) M = Nb, and (c) M = Ta.

materials showed a single resonance at ca. 3369−3380 G approximately 5 G wide with an absence of any hyperfine coupling for even dilute samples. This observation is consistent with a free electron in the wall of the material only loosely bound to a localized Mn-d (M = Ti, Nb, Ta) state or a material with a broad distribution of sites as expected in an amorphous material. Since changing either the alkali metal dopant or the transition metal in the mesostructured framework had little effect on the position of this signal, the free-electron formulation seems likely in these materials, although this does not explain the trend toward decreasing binding energy with increasing molecular weight of dopant in the XPS spectra, which suggests a more intimate interaction between the reducing electron and the transition metal center. However, this does not necessarily rule out a broad distribution of reduced site morphologies as would be expected from a material with an amorphous structure. Thus, the techniques used in this study are not entirely able to describe the subtle electronic effects at play in these systems.

3.5. Electrochemical Studies. To probe further into the electrochemical nature of unreduced mesoporous Nb, Ta, and

Ti oxides we conducted a series of cyclic voltamograms (CVs) at 50, 100, and 200 mV. The reversibility of electron transfer in these materials is an extremely important feature in designing nanoscale electronic devices. Figure 11 shows the CV for all three materials at 100 mV/s. The CV run for the Ti material (Figure 11a) showed clear peaks at 0.8 and 1.4 V indicating reversible reduction of the oxide framework. Because of this facile reversibility, this material may have applications in fuel cell fabrication where catalytic substrates capable of harnessing and transferring electrical energy are required. The Nb material showed weak peaks at 0.9 and 1.5 V (Figure 11b) with the rectangular shape associated with a capacitor beginning to emerge. Figure 11c shows the CV of the Ta material. There is a small peak at 0.9 V with no evidence of a reversible process and an overall rectangular shape due to the strong capacitance of this material. Samples of amorphous oxides Ti, Nb and Ta oxides prepared by precipitation at pH 5 from metal alkoxides and water followed by aging in water at 100 °C for 10 days afforded CVs that were virtually identical to those of the corresponding mesoporous oxide, demonstrating that the mesostructured nature of these materials had little effect on their electrochemical behavior. Comparisons of these values with known half-cell values of the crystalline oxides[42] are not meaningful since reduction potential is known to vary greatly with ligand-field environment and crystal structure of the material. The high capacitance of the Nb and Ta materials is expected due to the insulating nature of these materials and suggests that they may have applications as supercapacitors. The difference in electrochemical behavior of the Ti, Nb, and Ta materials can be explained by differences in capacitance and electron transport through the oxide. Nb-TMS1 and Ta-TMS1 are highly insulating, even when chemically reduced, and hence these materials show strong capacitance with little sign of electrochemical reduction. In contrast, chemically reduced Ti-TMS1 is conducting and because of this reversible electrochemical reduction proceeds more smoothly with little evidence for capacitance and electron transport problems. The CVs run at lower scan rates show weaker peaks as expected. The broadness of the oxidation−reduction peaks from all CVs in this study is consistent with the amorphous nature of the material leading to a broad distribution of reduction potentials. In other work we have already exploited this feature of these materials, as mesoporous niobium oxide is partially reduced by cobaltocene[35] or bis-benzene chromium,[36] reagents which do not react with bulk Nb_2O_5.

4. Conclusion

In conclusion, we have investigated a series of reduced mesoporous transition metal oxides to determine the effect of changing the alkali metal on the electronic and magnetic properties of the material. While the Nb and Ta materials are insulating and show promise as capacitors, the high conductivity and reversible oxidation−reduction of the Ti materials warrant further study in future applications where high surface area electron storage materials are required. The high surface area and potential for fast diffusion in these materials also suggests that they might find applications as fast ion conduction channels. Ion conductivity and Li NMR studies are ongoing in our group with the view in mind of further probing the physical properties and applications of these new materials.

Acknowledgment. NSERC and The Ontario Premier's Research Excellence Award program are thanked for funding. Maryam and Abbas Nazri are thanked for their help in electrochemistry, and Xun He is thanked for his help with EPR studies.

IC0011359

(41) Bruce, P. G. *Solid State Electrochemistry*; Cambridge University Press: Cambridge, 1995.
(42) Seki, S.; Unagami, T.; Kogure, O. *J. Electrochem. Soc*. **1985**, *132*, 3054.